Electronic Supplementary Material (ESI) for Journal of Materials Chemistry A.

Supporting Information

Construct 3D MoS_2 Superspheres with Quasi Molecular Superlattices: In-situ Anion-exchange Formation and and Li-storage properties

Feilong Gong, Lifang Peng, Huanzheng Liu, Yonghui Zhang, Dianzen Jia, Shaoming Fang, Feng Li* and Dongming Li*

*Corresponding author. Tel.: +86 136 7399 6373.
E-mail address: fengli@zzuli.edu.cn; lifeng696@yahoo.com; doli@utmb.edu

1. The photo of particles produced at different temperature

Figure S1. The photo of S160, S180, S200 and S220 of *ca*. 2 g each produced at 160, 180, 200 and 220 °C, respectively. The color of the materials changes from yellow to black as elevating reaction temperature.

The colors of the materials vary in corresponding to the reaction temperature, which indicates the composition evolution of the materials.

2. The HRTEM studies on the inner core of the core-shell supersphere

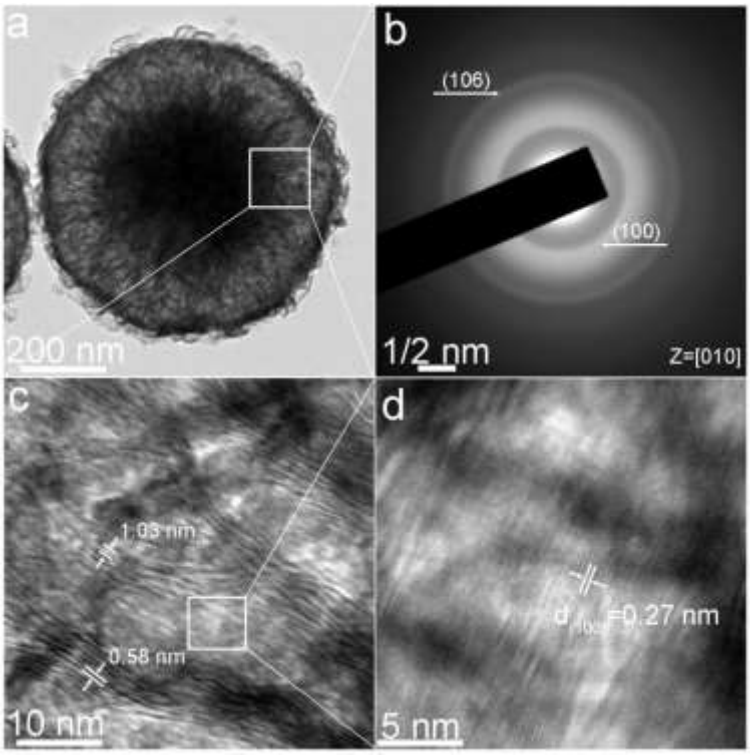

Figure S2. (a) The TEM image of a S220 supersphere. (b) The SAED pattern and HRTEM image collected at the area highlighted with white square in (a). (d) The HRTEM image at the area highlighted with white square in (c).

The HRTEM images clearly reveal the lattices with d-spacings of ~1.03, 0.58 and 0.27 nm in the inner core areas of the superspheres, corresponding to the molecular superlattice, (002) and (100) planes of MoS_2, respectively. The SAED pattern collected at the inner core also show polycrystalline diffraction rings ascribed as (106) and (100) facets of MoS_2 with [010] zone axis. The core-shell superspheres consist of 2D MoS_2 nanosheets with quasi molecular superlattices.

3. The SEM images of particles prepared at different temperatures

Figure S3 shows the FESEM images and size distributions of S160, S180, S200 and S220 prepared at 160, 180, 200 and 220 °C, respectively. The particles of 1050 ± 230, 915 ± 77, 815 ± 53 and 780 ± 48 nm in diameters can be produced successfully on gram scales. The size of the superspheres becomes smaller, after performing the reaction at higher temperature. It can be observed obviously that the surfaces of the superspheres change dramatically from relatively smooth to rough and bumpy for the formation of oriented nanosheets. The superspheres eventually self-focus their size on 780 ± 48 nm.

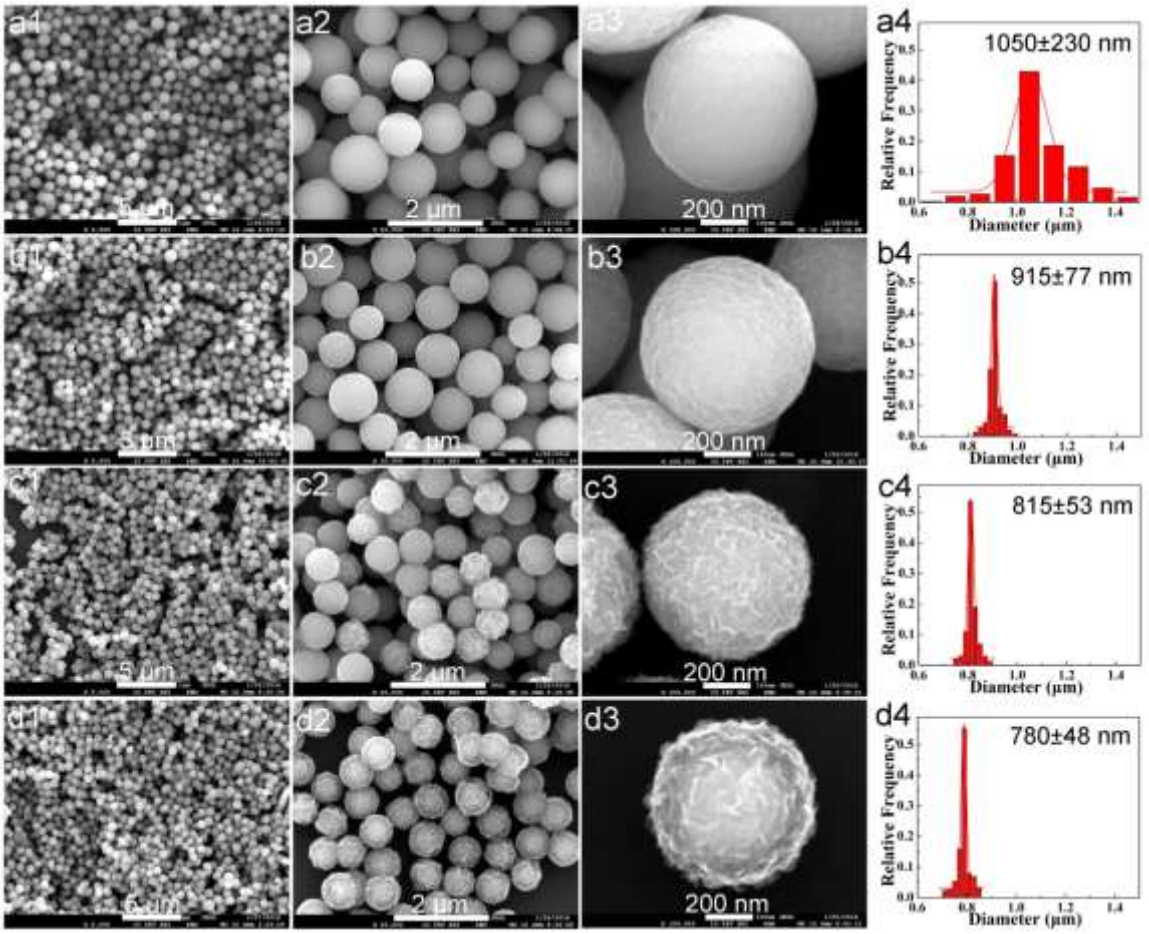

Figure S3. FESEM images of S160, S180, S200 and S220 obtained at (a1 - 3) 160, (b1 - 3) 180, (c1 - 3) 200 and (d1 - 3) 220 °C, respectively. (a4 - d4) show the size distributions of the superspheres.

4. The XRD profiles of the materials synthesized

The XRD profiles of samples prepared at 160 and 180 °C, respectively, are similar. Most of the diffraction peaks can be indexed to both Mo_4O_{11} (JCPDS Card No. 05-0337) or MoO_2 (JCPDS Card No. 32-0671), because the diffraction peaks attributed to MoO_2 are very close to those of Mo_4O_{11}. The broadened peaks indicate that very small nanoclusters have formed inside the superspheres. A new peak appeared at low angle region of *ca*. 9.0 Å, which is twice of 4.5 Å, can be considered as the multiple frequency peak of (401) plane of Mo_4O_{11}. In contrast, new diffraction peaks attributed to (100) and (106) facets of MoS_2 (JCPDS Card No. 37-1492) appear in the XRD profile of sample synthesized at 200 °C, while the weakened diffraction peaks belonged to Mo_4O_{11} and MoO_2 still exist. After performing the reaction at 220 °C, however, the diffraction peaks attributed to Mo_4O_{11} and MoO_2 disappear in the XRD profile of the materials, and all of the diffraction peaks can be indexed to MoS_2 (JCPDS Card No. 37-1492). Interestingly, a diffraction peak with d-spacings of 11.3 Å in the XRD profiles of materials produced at 200 and 220 °C can be attributed to the formation of molecular superlattices, clearly indicating the formation of lamellar structures with enlarged interlayer spacings. The broadened diffraction peaks also confirm the small grain size of the materials.

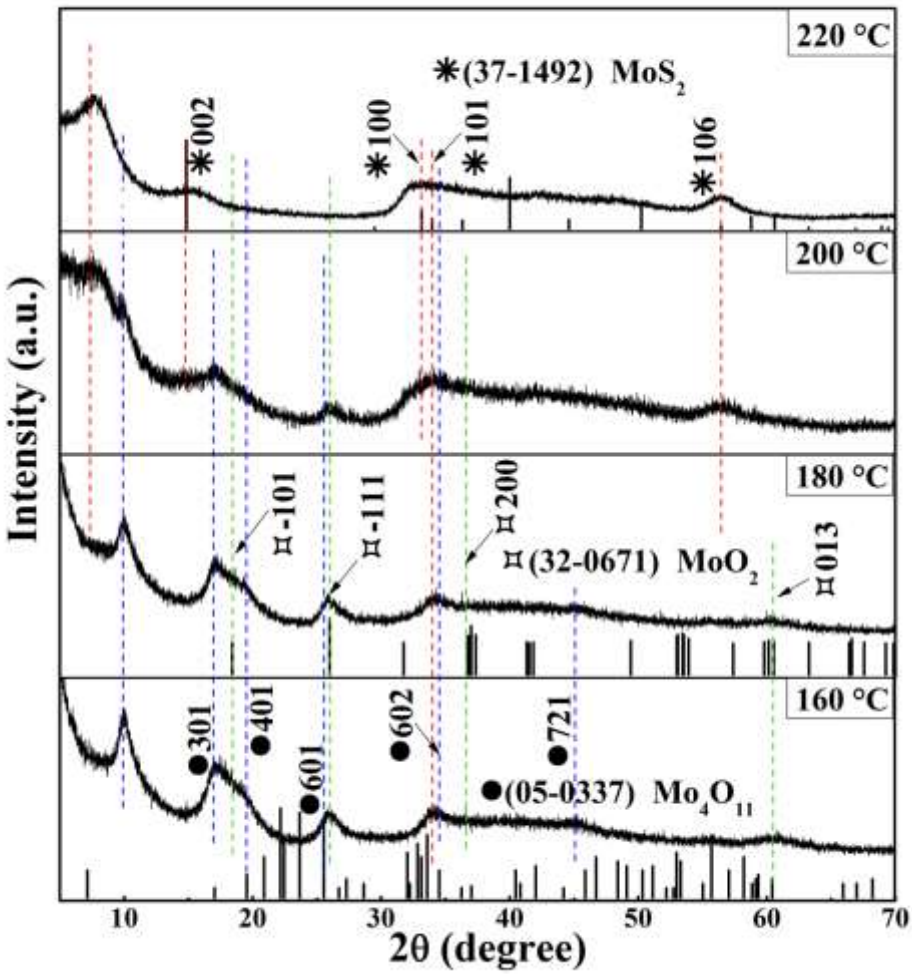

Figure S4. XRD profiles of S160, S180, S200 and S220 produced at 160, 180, 200 and 220 °C, respectively.

5. The BET analysis of the materials

The BET surface areas (Figure S4a) of S160, S180, S200 and S220 prepared at 160, 180, 200 and 220 °C are 5.9, 11.5, 56.7 and 159.2 m^2g^{-1}, respectively. The average pore diameters (Figure S4b) of the materials are 11.04, 7.79, 7.27 and 8.91 nm, respectively.

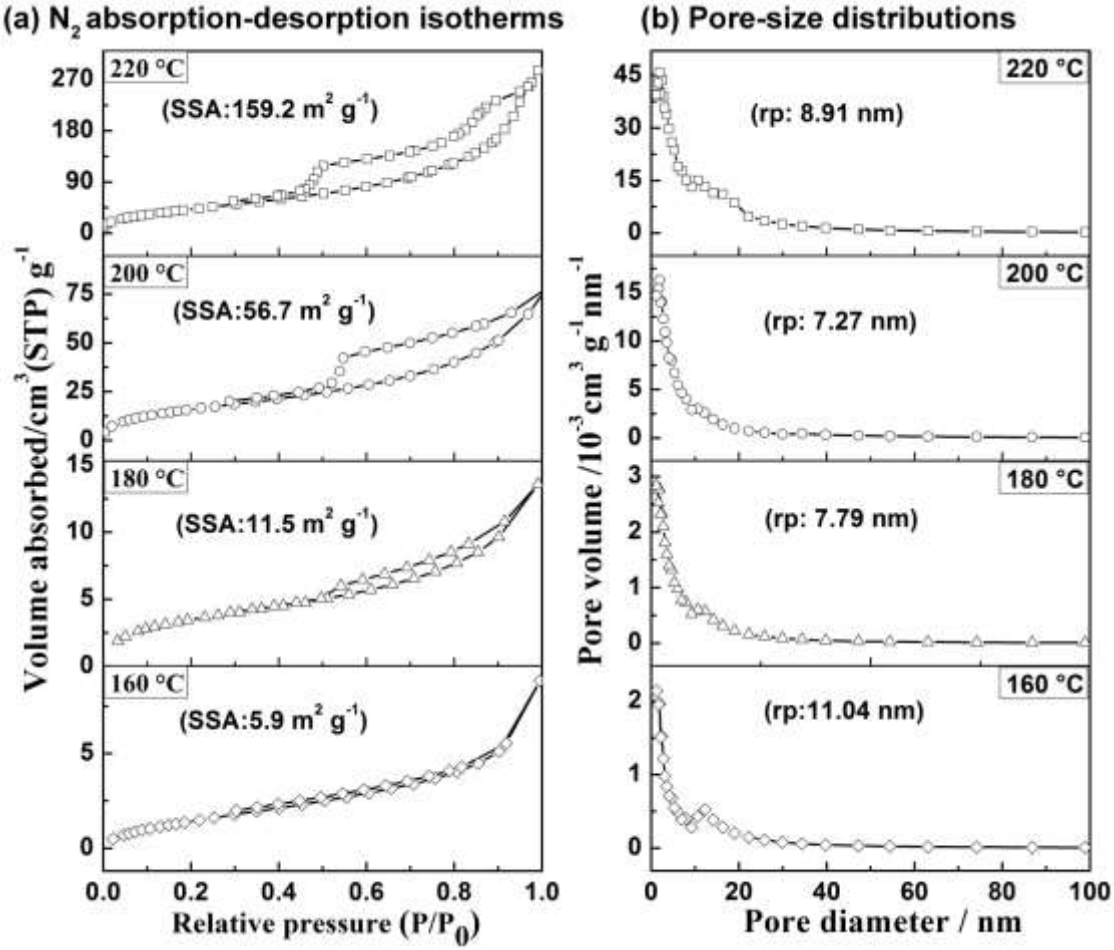

Figure S5. (a) Physisorption isotherms and (b) pore-size distributions of S160, S180, S200 and S220 prepared at 160, 180, 200 and 220 °C, respectively. *SSA* and *rp* represent the specific surface area and average pore size, respectively.

6. The EDS profiles of superspheres prepared at different temperature

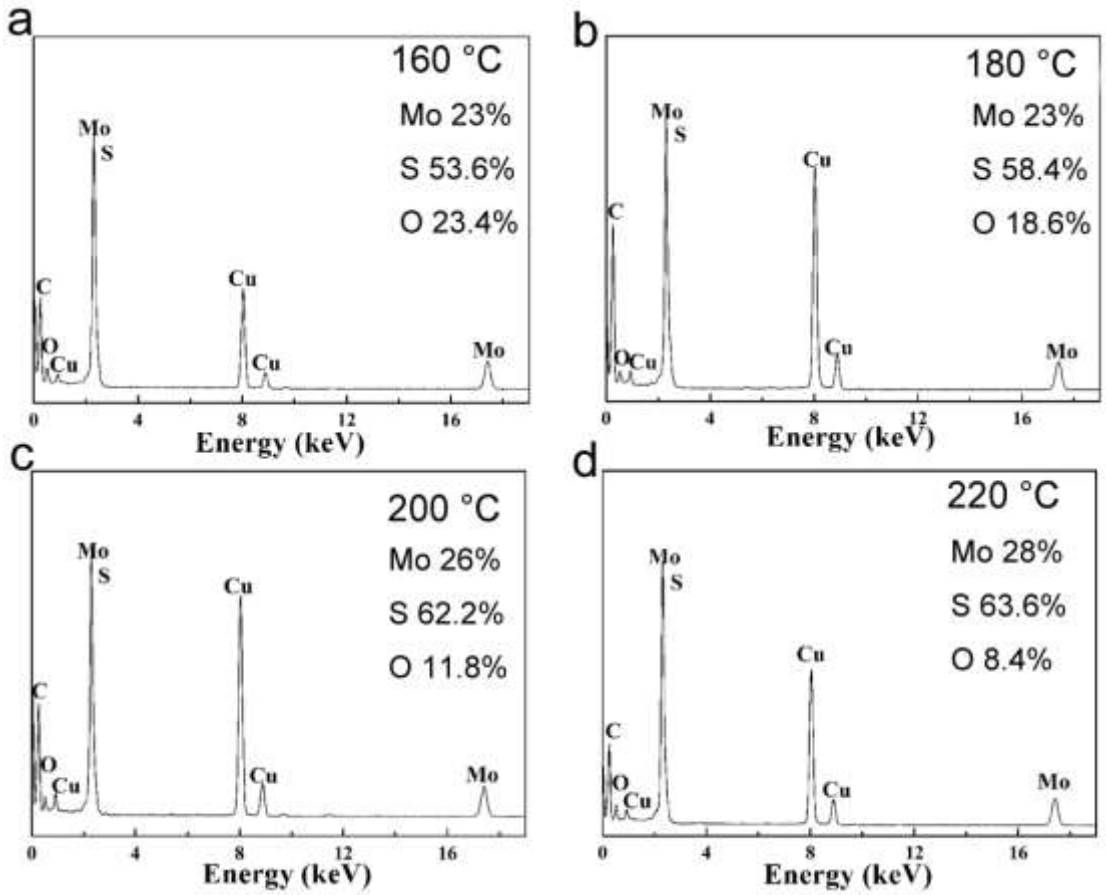

Figure S6. EDS profiles of of S160, S180, S200 and S220 prepared at 160, 180, 200 and 220 °C, respectively. Compared to the gradual decrease of O element concentrations, the molar ratio of S to Mo keeps at a value higher than 2:1, as elevating reaction temperature from 160 to 220 °C.

7. The XPS analyses of as-prepared materials

The XPS surveys of S160, S180, S200 and S220 prepared at 160, 180, 200 and 220 °C, respectively, as well as thiourea, were presented in Figure S6. The peaks belonging to Mo 3p, Mo 3d, S 2p and O 1s can be observed in the surveys. All of the spectra were calibrated with the C 1s peak located at 284.80 eV.

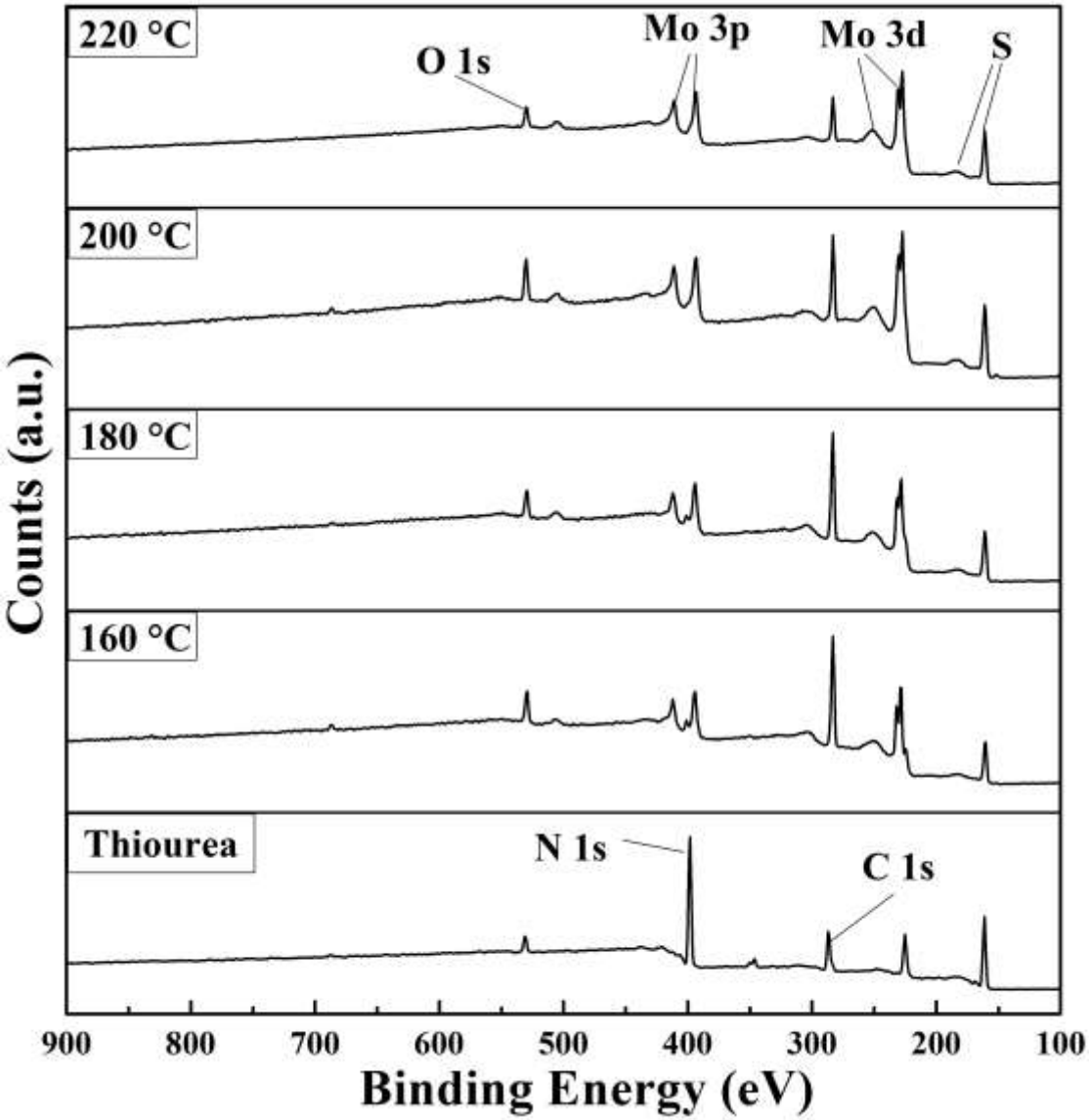

Figure S7. The XPS surveys of thiouea and materials prepared at 160, 180, 200 and 220 °C, respectively.

The high-resolution XPS spectra of O element are depleted in Figure S7. The peaks at 530.82 and 531.2 eV can be attributed to O1s of MoO_2 (red line) and Mo_4O_{11} (blue line), respectively. In addition, the peak located at 532.25 eV can be ascribed to adsorbed oxygen including water and -OH. The Mo-based oxide (MoO_x) mainly exists as Mo_4O_{11} in the materials prepared at 160 °C and it converts to MoO_2 gradually at higher reaction temperature. It can be found that the concentration of O element decreases dramatically with elevating the reaction temperature.

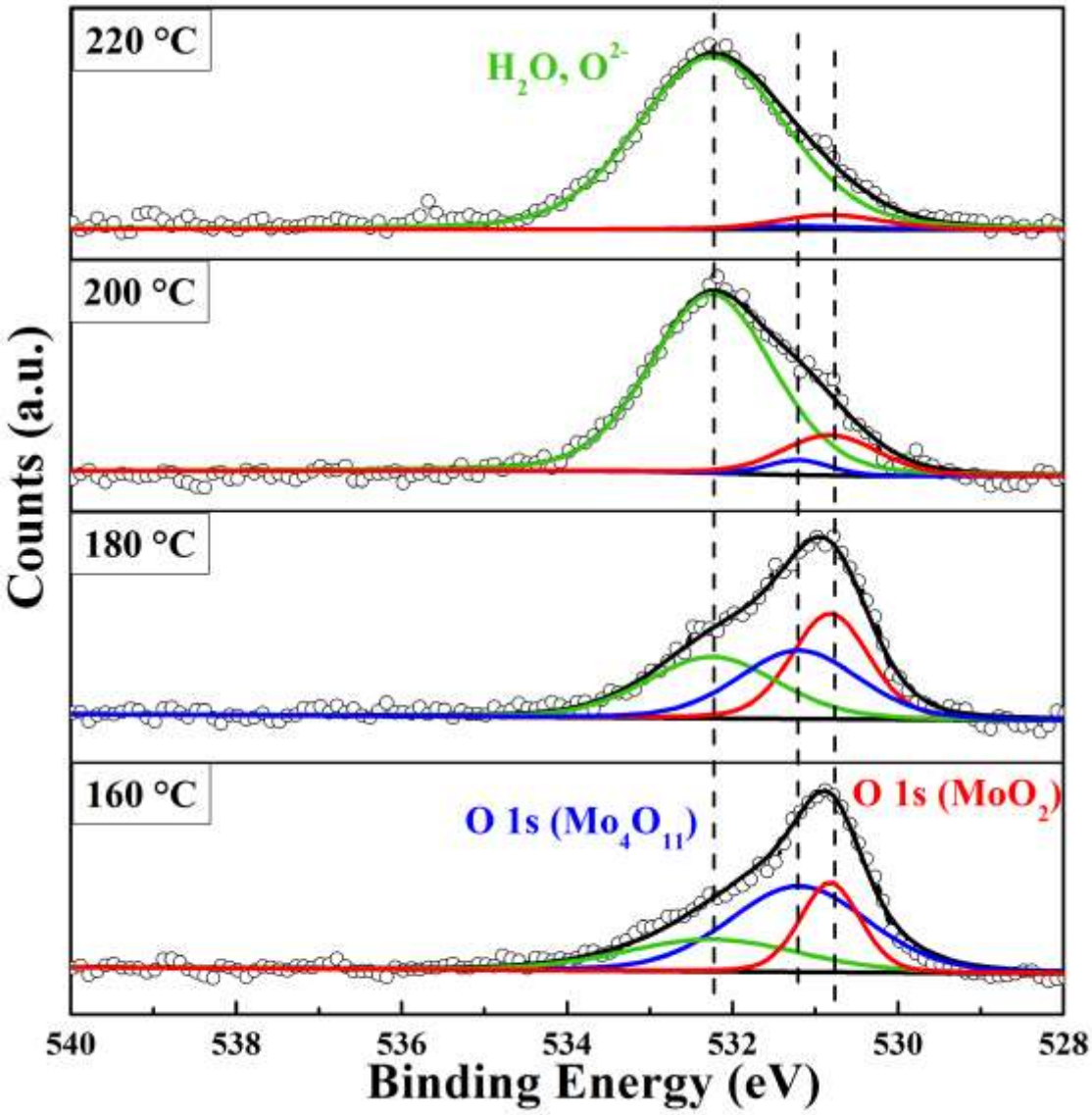

Figure S8. The high-resolution XPS spectra of O element in S160, S180, S200 and S220 synthesized at 160, 180, 200 and 220 °C, respectively.

The high-resolution XPS spectra of N 1s are shown in Figure S8. The peak attributed to C-N bond at 399.3 eV (green line) of thiouea is very strong in its XPS spectrum, and it weakens and shifts to 399.69 eV for the decomposition of thiourea after performing the reaction at temperature higher than 160 °C. The $Mo^{5.5+}$ 3p (396.03 eV) peak also becomes weaker with increasing the reaction temperature, in contrast to the Mo^{4+} 3p peak located at 394.77 eV (red line) becoming stronger. The results indicate that reactant thiouea has already decomposed at 160 °C, and the $Mo^{5.5+}$ cations in the materials can be reduced to Mo^{4+}, which is consistent with the results from XPS spectra of S 2p and Mo 3d.

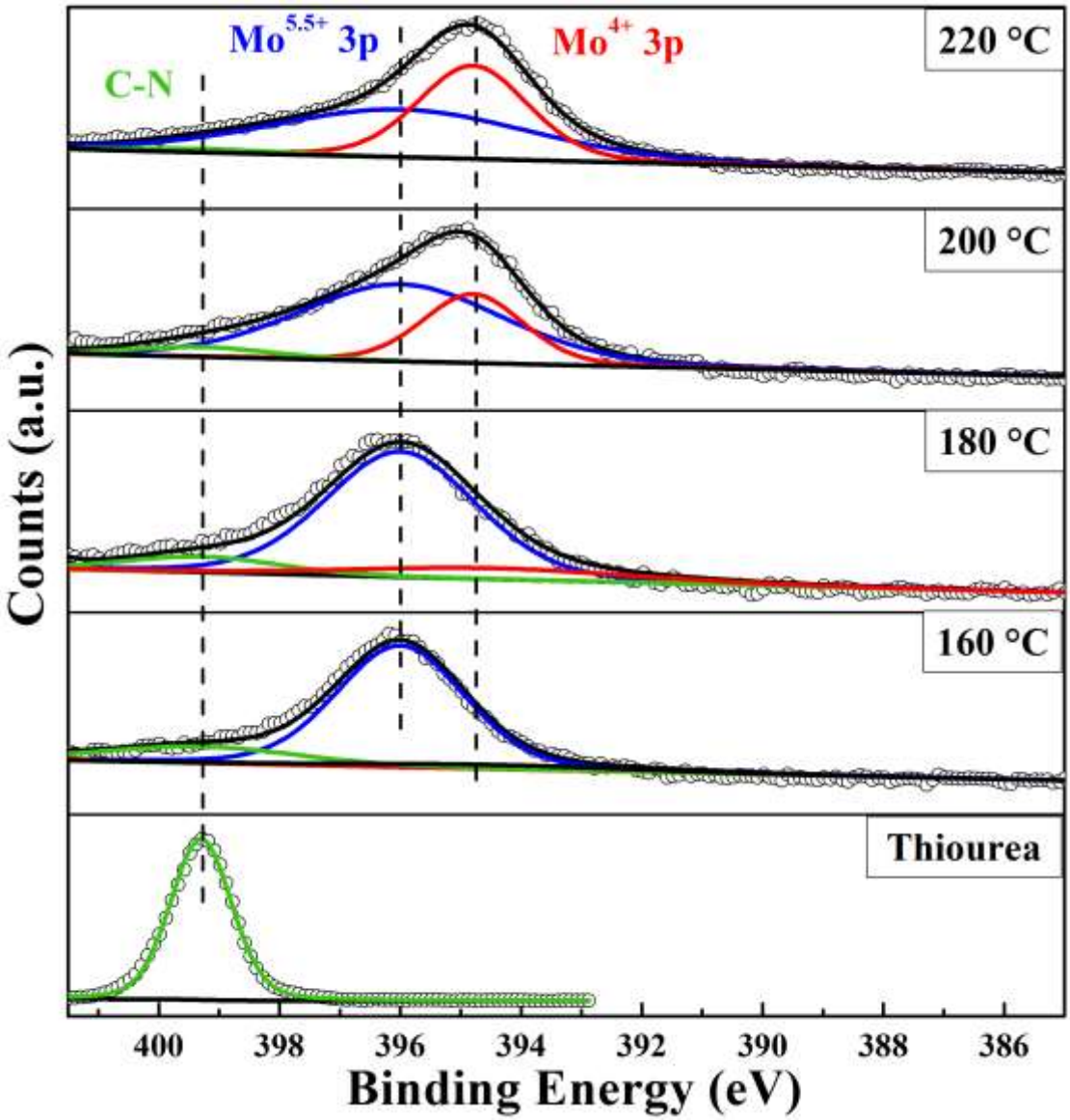

Figure S9. The high-resolution XPS spectra of N element in S160, S180, S200 and S220 synthesized at 160, 180, 200 and 220 °C, respectively.

8. The composition and chemical state evolutions of as-prepared materials

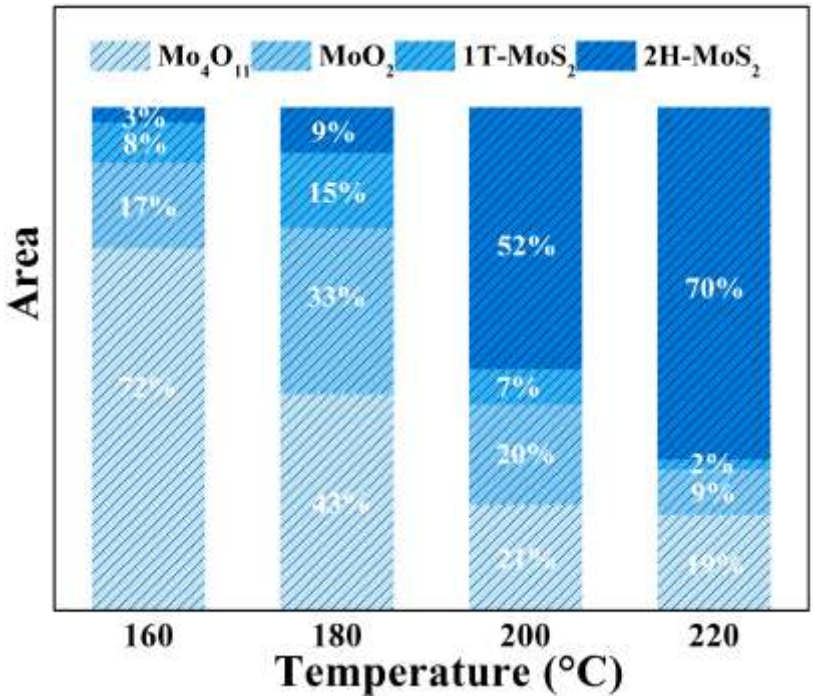

Figure S10. The composition and chemical state evolutions on the surfaces of S160, S180, S200 and S220, calculated based on the areas of each component in the core-level Mo $3d_{5/2}$ and Mo $3d_{3/2}$ XPS spectra.

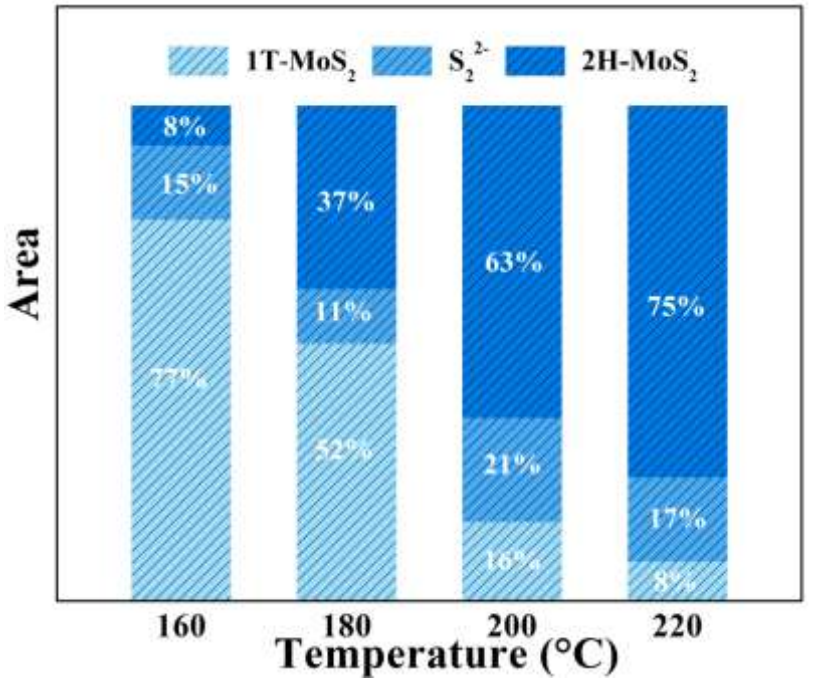

Figure S11. The composition and chemical state evolutions on the surfaces of S160, S180, S200 and S220, calculated based on the areas of each component in the core-level S 2p high resolution XPS spectra.

9. The TG curves of S160, S180, S200 and S220

The TG curves show that the materials prepared at 160, 180, 200 and 220 °C lose 29.4%, 28.1%, 20.1% and 15% of their weights, respectively, at *ca*. 300 °C.

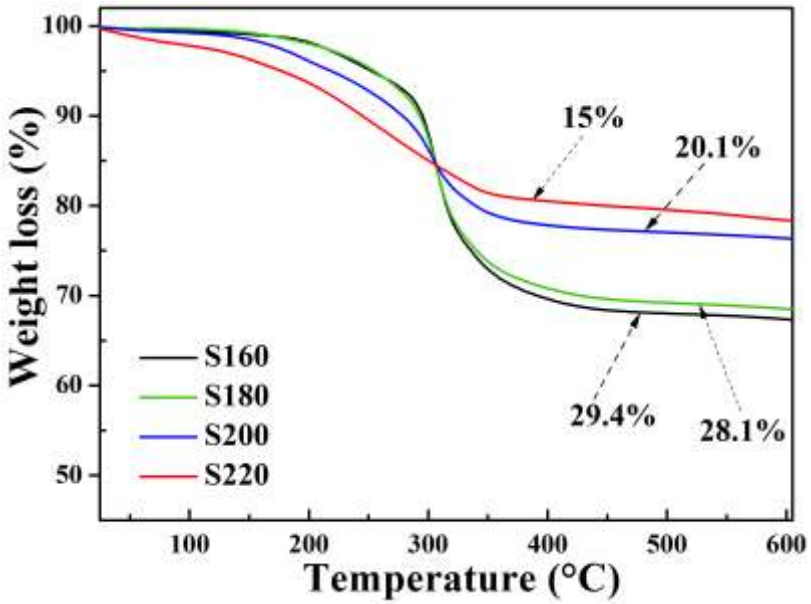

Figure S12. TG curves of the products obtained at 160, 180, 200 and 220 °C, respectively.

10. The FT-IR spectra of as-prepared materials and related chemicals

In the FT-IR spectrum of thiourea, the peaks located at 625, 1605, 3150-3365 cm^{-1} in the FT-IR spectra can be ascribed to the symmetric stretching, asymmetric stretching, and symmetric stretching vibrations of N-H, respectively. The bands located at 726 and 1407 cm^{-1} are attributed to the symmetric and asymmetric stretching of C=S vibrations, and the 1083 and 1466 cm^{-1} bands belong to the C-N and N-C-N symmetric stretching vibration. In the FT-IR spectrum of CTAB, the peaks at 718-731, 913-962, 1460 and 1492, 2848-2920 cm^{-1} are attributed to the $-CH_2-$ rocking mode vibration, $C-N^+$ stretching vibration of CH_3-N^+, C-H symmetric and asymmetric vibration of CH_3-N^+, and C-H symmetric and asymmetric vibration, respectively. In the FT-IR spectrum of Na_2MoO_4 (Figure S13), the characeristic absorption peaks are located at 799, 912, 853, 899 and 1674-1704 cm^{-1}, reapectively. The FT-IR spectrum of the micromicelles, which were prepared with CTAB, thiourea and Na_2MoO_4 at room temperature, consists of broadened peaks attributed to N-H, C-H, C-O, C-N, C-N-C, O-H, Mo-O and Mo=O bonds, respectively. After incubated at 160 °C, however, the FT-IR spectrum of S160 mainly consists of C-H, C-N, Mo-O and Mo=O vibrations. In contrast, the vibrations attributed to C=S and N-H bonds disappear in the spectrum. After further elevating the reaction temperature, vibrations attributed to Mo-S (649, 1032 and 1404-1406 cm^{-1}) and Mo=S (908 and 1508 cm^{-1}) bonds appear in the FT-IR spectra, and the intensities of peaks belonged to C-H, Mo-O and Mo=O bonds decrease dramatically. The detailed information concerned with FT-IR spectra of the superspheres and related raw materials is summarized in Table S1. The results indicate that CTAB molecule exists in all of as-produced materials, while reactant thiourea decomposes in the the reaction at temperature higher than 160 °C.

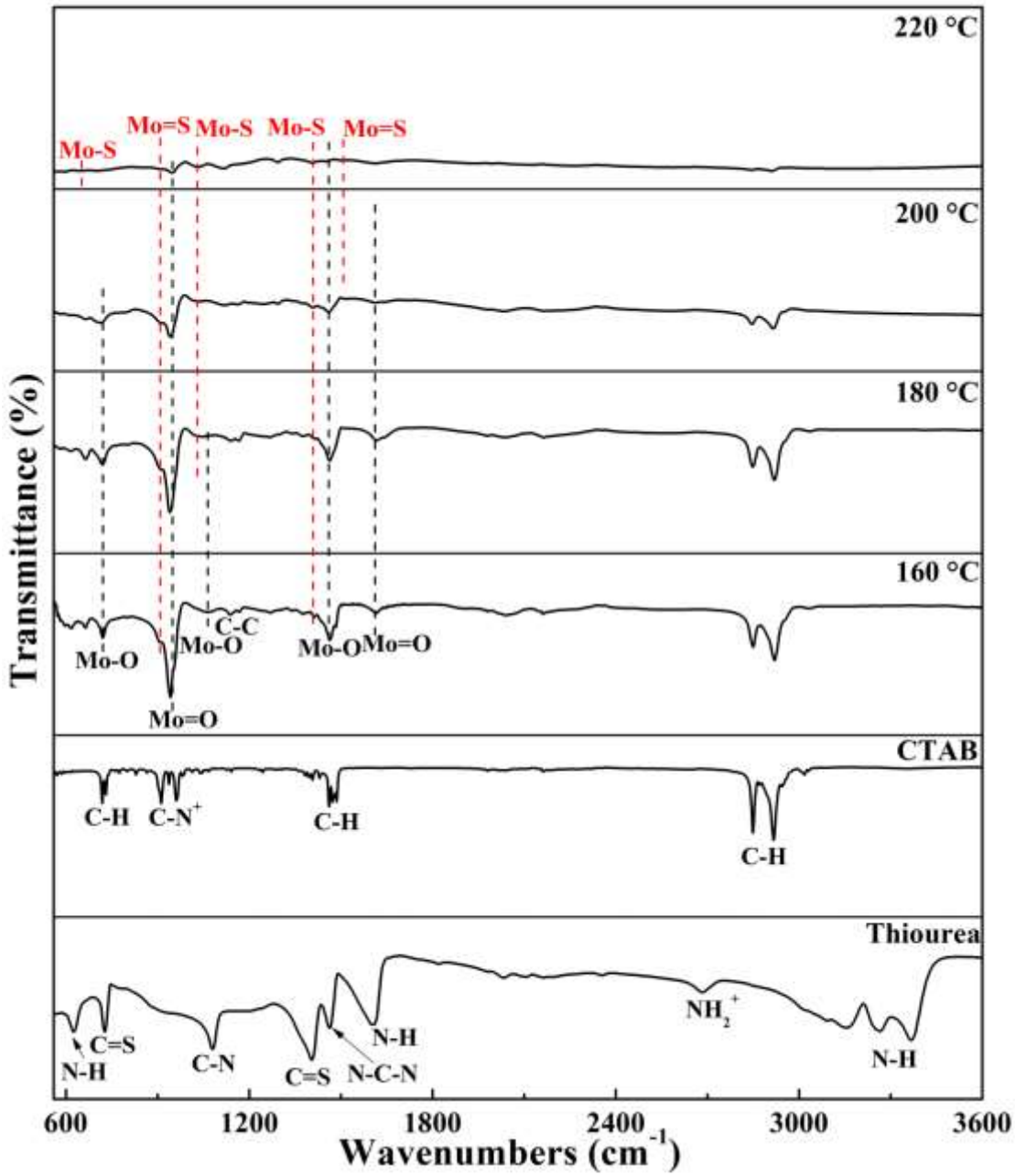

Figure S13. FT-IR spectra of S160, S180, S200, S220, thiourea and CTAB.

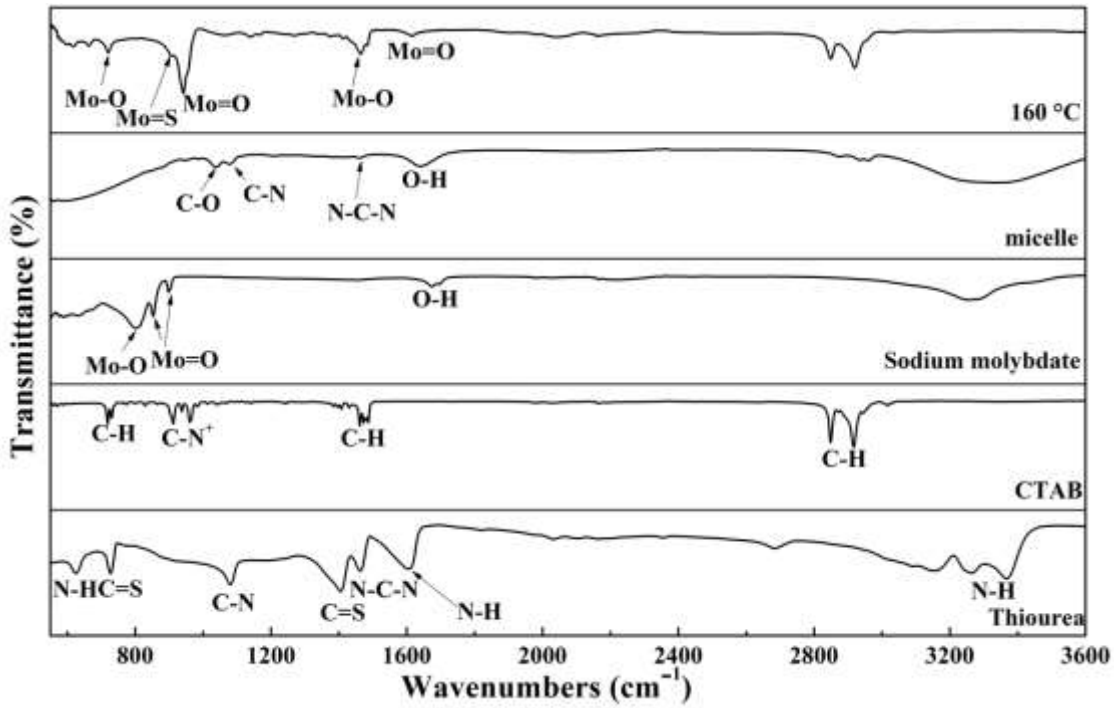

Figure S14. FT-IR spectra of thiourea, CTAB, Na_2MoO_4, micromicelles and S160.

Table S1. FT-IR absorption bands of thiourea, CTAB, Na_2MoO_4, micromicelle, S160, S180, S200 and S220.

	Thiourea	CTAB	Na_2MoO_4	micelle	S160	S180	S200	S220
N-H	625 (s) 1605 (s) 3150-3365 (s)	-	-	3310 (w)	-	-	-	-
C-H	-	718-731 (s) 1460-1492 (s) 2848-2920 (s)	-	2873-2962 (w, b)	2848-2920 (s)	2848-2920 (s)	2848-2920 (s)	2848-2920 (w)
C=S	726 (s) 1407 (s)	-	-	-	-	-	-	-
C-S	-	-	-		663 (w)	663 (w)	663 (w, b)	-
C-O	-	-	-	1040 (w)			-	-
S-S	-	-	-	-	-	-	-	-
C-N	1083 (s) 1466 (s)	913-962 (s)	-	1082 (w) 1466 (w)	1466 (sh)	-	-	-
O-H	-	-	1674-1704 (w, b), 3236-3300 (w, b)	1641 (b), 3338 (w, b)	-	-	-	-
Mo=O	-	-	853 (w) 899 (w)	<910 (b)	942 (s), 1612 (w)	942 (s), 1612 (w)	942 (s), 1612 (w)	948 (w), 1612 (w)
Mo-O	-	-	799 (b) 812 (sh)	<910 (b)	720 (s), 1054, 1470 (s)	720 (s) , 1054 (w), 1462 (s)	711 (w, b), 1462 (s)	1460 (w)
Mo-S					1406 (w)	1032(w), 1404 (w)	1032(w), 1404 (w)	649 (w), 1032(s), 1404 (w)
Mo=S	-	-	-	-	908 (w, sh)	908 (w, sh)	908 (w, sh), 1508 (w, b)	908 (w, sh), 1508 (w, b)

* s = strong; w = weak; b = broaden; sh = shoulder

11. The XRD profile and Raman Spectra of S220A

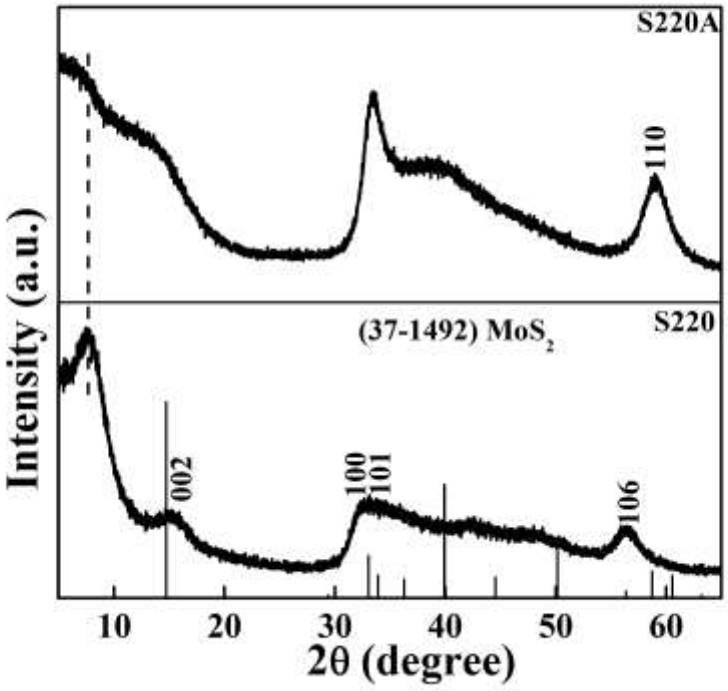

Figure S15. The XRD profiles of S220A and S220.

The XRD profiles shown in Fig. S15 reveal that all of the diffraction peaks in the XRD profile of S220A become sharper and stronger in comparison with those of S220. Notably, the peak ascribed to CTAB-MoS_2 molecular superlattices at 7.5 degree weakens and becomes wide, after annealed at 350 °C. The presence of CTAB in the materials could result in the materials

peeling of the electrodes. In addition, the diffraction attributed to (106) plane of MoS_2 disappears, while the peak corresponding to (110) facets arises.

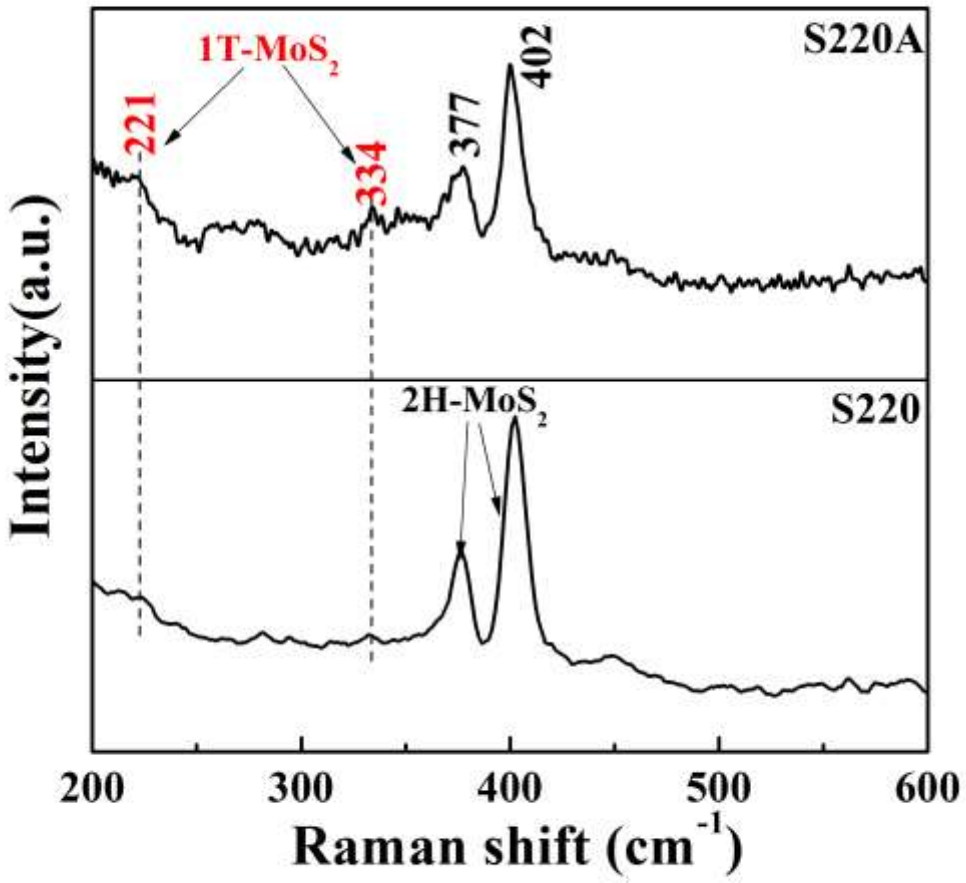

Figure S16. The Raman spectra of S220A and S220.

The Raman spectra (Fig. S16) of the materials are also collected to characterize their composition, after annealed. The A1g and E2g peaks belonged to 2H-MoS2 at 377 and 402 cm^{-1} indicate that 2H-MoS_2 is the main component of the materials, after calcination at 350 °C. Meanwhile, the relative intensities of two weak peaks located at 221 and 334 cm^{-1} become stronger in the spectra, suggesting the formation of more mental phase of MoS_2 (1T-MoS_2). Some of the 2H-MoS_2 converts into 1T phase after calcination.

12. Electrochemical performance of S220A

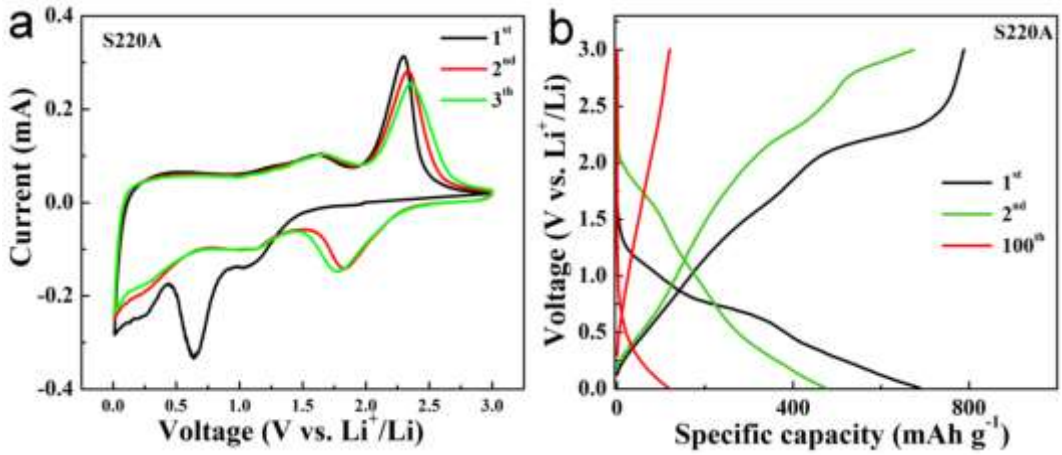

Figure S17. (a) Cyclic voltammograms at a scanning rate of 0.1 mV/s during the first three cycles and (b) typical voltage versus specific capacity profiles for the first, second and 100th discharge/charge cycles of S220A at current density of 200 mA g^{-1}.

13. The structural stability of S220A in anode

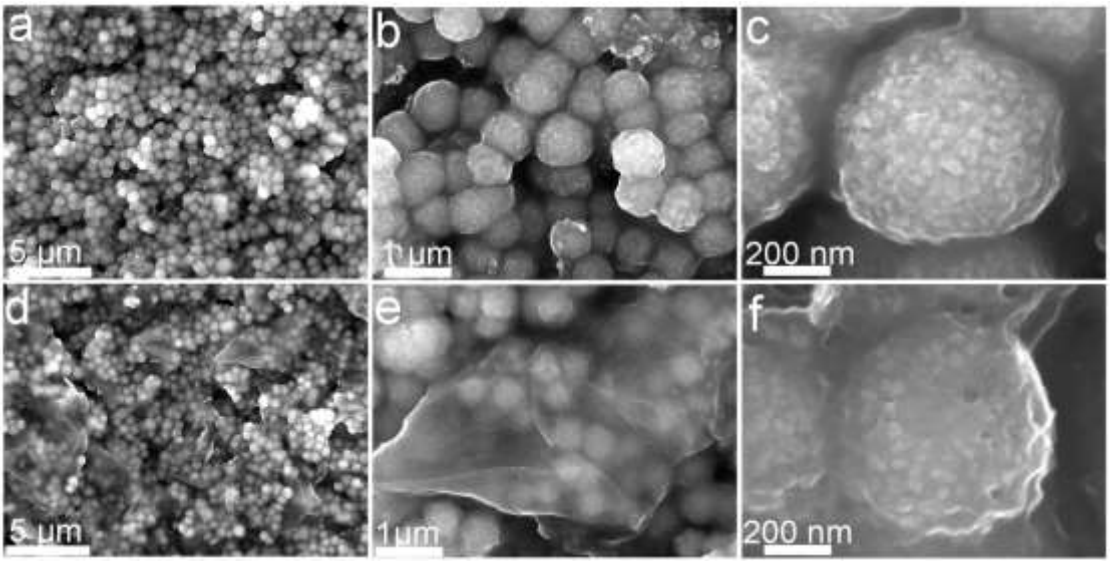

Figure S18. The FESEM images of (a-c) S220A and (d-f) S220A@GRO electrodes after cycling for 100 times at 1 A g^{-1}.

We have dismantled the coin cells made with S220A and S220A@RGO, respectively, and investigated their structures with FESEM, after cycling for 100 times at 1 A g^{-1}. Specially, the superspheres in both S220A and S220A@RGO electrodes can keep their 3D spherical structures, indicating their excellent structural stability. However, the FESEM images at higher magnification as shown in Fig. S18c and S18f reveal that the 2D nanosheets on the surfaces of the superspheres transform to nanoparticles of about 50 nm after cycling for 100 times at 1 A g^{-1}. The nanostructural changes could be resulted from the lithiation and reactions taking place during charge-discharge process. The results indicate that the 3D core-shell structure assembled with nanosheets can effectively buffer the volume change during lithiation.